

# Image patterned molecular delivery into live cells using gold particle coated substrates

Ting-Hsiang Wu,<sup>1</sup> Sheraz Kalim,<sup>2</sup> Caitlin Callahan,<sup>2</sup> Michael A. Teitell,<sup>2,\*</sup>  
and Pei-Yu Chiou<sup>3,\*</sup>

<sup>1</sup>Department of Electrical Engineering, University of California, Los Angeles (UCLA), 420 Westwood Plaza,  
48-121 Engineering IV, Los Angeles, CA 90095-1597, USA

<sup>2</sup>Departments of Pathology and Pediatrics, UCLA, 675 Charles E. Young Drive South, MRL 4-762,  
Los Angeles, CA 90095-1732, USA

<sup>3</sup>Department of Mechanical and Aerospace Engineering, UCLA, 420 Westwood Plaza, 48-121 Engineering IV,  
Los Angeles, CA 90095-1597, USA

\*[pychiou@seas.ucla.edu](mailto:pychiou@seas.ucla.edu)

**Abstract:** An image-patterned molecular delivery system for mammalian cells is demonstrated by pulsed laser irradiation of gold particles immobilized on a substrate below a cell monolayer. Patterned cavitation bubble nucleation was captured using a time-resolved imaging system and molecular delivery verified by observing the uptake of a membrane-impermeable fluorescent dye, calcein. Delivery efficiency as high as 90% was observed and multiplexed, patterned dye delivery was demonstrated.

©2009 Optical Society of America

OCIS codes: (140.3540) Lasers, Q-switched; (170.1420) Biology; (170.1530) Cell analysis.

---

## References and links

1. A. Vogel, J. Noack, G. Hüttman, and G. Paltauf, "Mechanisms of femtosecond laser nanosurgery of cells and tissues," *Appl. Phys. B* **81**(8), 1015–1047 (2005).
2. U. K. Tirlapur, and K. König, "Targeted transfection by femtosecond laser," *Nature* **418**(6895), 290–291 (2002).
3. C. M. Pitsillides, E. K. Joe, X. Wei, R. R. Anderson, and C. P. Lin, "Selective cell targeting with light-absorbing microparticles and nanoparticles," *Biophys. J.* **84**(6), 4023–4032 (2003).
4. C. Yao, R. Rahmzadeh, E. Endl, Z. Zhang, J. Gerdes, and G. Hüttmann, "Elevation of plasma membrane permeability by laser irradiation of selectively bound nanoparticles," *J. Biomed. Opt.* **10**(6), 064012 (2005).
5. V. Kotaidis, C. Dahmen, G. von Plessen, F. Springer, and A. Plech, "Excitation of nanoscale vapor bubbles at the surface of gold nanoparticles in water," *J. Chem. Phys.* **124**(18), 184702 (2006).
6. S. J. Henley, J. D. Carey, and S. R. P. Silva, "Pulsed-laser-induced nanoscale island formation in thin metal-oxide films," *Phys. Rev. B* **72**(19), 195408 (2005).
7. J. Trice, D. Thomas, C. Favazza, R. Rueshikumar, and R. Kalyanaraman, "Pulsed-laser-induced dewetting in nanoscopic metal films: Theory and experiments," *Phys. Rev. B* **75**(23), 235439 (2007).
8. E. D. Tsagarakis, C. Lew, M. O. Thompson, and E. P. Giannelis, "Nanocrystalline barium titanate films on flexible plastic substrates via pulsed laser annealing," *Appl. Phys. Lett.* **89**(20), 20910 (2006).
9. C. F. Bohren, and D. R. Huffman, *Absorption and Scattering of Light by Small Particles* (Wiley, New York, 1983).
10. P. Mulvaney, "Surface plasmon spectroscopy of nanosized metal particles," *Langmuir* **12**(3), 788–800 (1996).
11. C. E. Brennen, "Phase change, nucleation and cavitation," in *Cavitation and Bubble Dynamics*, (Oxford University Press, New York, 2005).
12. G. Mie, "Articles on the optical characteristics of turbid tubes, especially colloidal metal solutions," *Ann. Phys. (Leipzig)* **25**, 377 (1908).
13. P. K. Jain, K. S. Lee, I. H. El-Sayed, and M. A. El-Sayed, "Calculated absorption and scattering properties of gold nanoparticles of different size, shape, and composition: applications in biological imaging and biomedicine," *J. Phys. Chem. B* **110**(14), 7238–7248 (2006).
14. P. B. Johnson, and R. W. Christy, "Optical constants of the noble metals," *Phys. Rev. B* **6**(12), 4370–4379 (1972).
15. H. Goldenberg, and C. J. Tranter, "Heat flow in an infinite medium heated by a sphere," *Br. J. Appl. Phys.* **3**(9), 296–298 (1952).
16. D. O. Lapotko, E. Lukianova, and A. A. Oraevsky, "Selective laser nano-thermolysis of human leukemia cells with microbubbles generated around clusters of gold nanoparticles," *Lasers Surg. Med.* **38**(6), 631–642 (2006).
17. I. B. Clark, E. G. Hania, J. Stevens, M. Gallina, A. Fieck, R. Brandes, B. O. Palsson, and M. R. Koller, "Optoinjection for efficient targeted delivery of a broad range of compounds and macromolecules into diverse cell types," *J. Biomed. Opt.* **11**(1), 014034 (2006).

## 1. Introduction

Optoporation, a method for molecule and gene delivery into cells, utilizes a tightly-focused, pulsed laser beam to create pores in the cell membrane [1]. It allows for contact-free delivery, and with the use of a femtosecond laser, high transfection efficiency that targets single cells has been demonstrated [2]. One drawback of this approach is that in order to obtain site-specific or patterned cell transfection, the laser beam must scan through every cell, which would be time consuming when large-scale, patterned cell transfection is desired, such as in complex tissues or in vitro with mixed co-culture systems.

An alternative contact-free method of increasing cell membrane permeability is to use light-absorbing micro- or nanoparticles [3]. Upon irradiation by a short pulse laser, the particles create transient and localized explosive bubbles, which disrupt part of the adjacent cell membrane leaving the remaining cell structure intact. By controlling the particle size, density and the laser fluence, cell permeabilization and transfection can be achieved with high efficiency [4]. Here we describe a device that can spatially select and target cells for molecular delivery by light image patterning. Large-scale, image-patterned molecular delivery could be enabled by this approach into specific cells within complex monolayer mixtures.

## 2. Device principle

The device consists of a glass substrate with gold particles immobilized on the surface (Fig. 1). Cells are seeded on this substrate until a confluent culture forms. A pulsed laser irradiates a shadow mask and the corresponding illumination pattern is imaged onto the substrate. In the area exposed to the pulsed laser, gold particles are heated to high temperatures due to the absorbed optical energy. Within nanoseconds, the heat is dissipated to the thin liquid medium layer surrounding the gold particles, which generates explosive vapor bubbles [5]. The rapid expansion and subsequent collapse of the vapor bubbles give rise to transient fluid flows, which induce strong shear stress on nearby adherent cells causing localized pore formation in the cell membrane. As a result, membrane-impermeable molecules can be carried into the cell by fluid flows or thermal diffusion. Since the cavitation bubble only takes place where the gold particle is exposed to the laser, an optical pattern can be designed to address molecular uptake in specified areas of the cell culture. This way high-throughput, spatially-targeted molecular delivery is made possible by controlling the gold particle size, density on the substrate, and the irradiation laser fluence.

To achieve fast and large-area immobilization of gold particles on the substrate, we utilized pulsed laser annealing of a thin gold film. The optical energy instantaneously melts the continuous gold film into discrete gold particles on the glass substrate. Mean particle size can be controlled by the thickness of the pre-annealed film [6]. The resultant high gold particle density ensures that every cell in a monolayer cell culture encompasses sufficient gold particles for reliable and effective molecular delivery.

## 3. Materials and methods

### 3.1 Pulsed laser annealing of gold films

The laser system is a Q-switched, frequency-doubled Nd:YAG laser at 532 nm in wavelength and 6 ns in pulsewidth (Continuum, Minilite I). The laser beam is linearly polarized and the pulse energy can be adjusted using a variable attenuator consisting of a half wave plate and a polarizing beam splitter. The pulse energy was measured using a pyroelectric optical energy detector (Newport, 1918-C). The sample was prepared by depositing a 10 nm thick gold film and a 1 nm titanium adhesion layer on a glass coverslip via electron beam evaporation. During pulsed laser annealing, the laser beam was sent through a holographic diffuser (Edmund Optics, NT55-848) and irradiated the gold film at a normal incidence. The diffuser reduces interference effects and smoothens the laser intensity profile. The laser spot, with a 3 mm diameter, scanned over the entire area of the gold film at a moving speed of 0.5 mm/sec. Using a laser pulse repetition rate of 10 Hz, the typical number of pulses received per unit

area was 60. After annealing, the sample morphology was inspected with a scanning electron microscope (Hitachi S4700 field emission SEM). The gold particle diameter and density were calculated using image analysis software (ImageJ, <http://rsbweb.nih.gov/ij/index.html>).

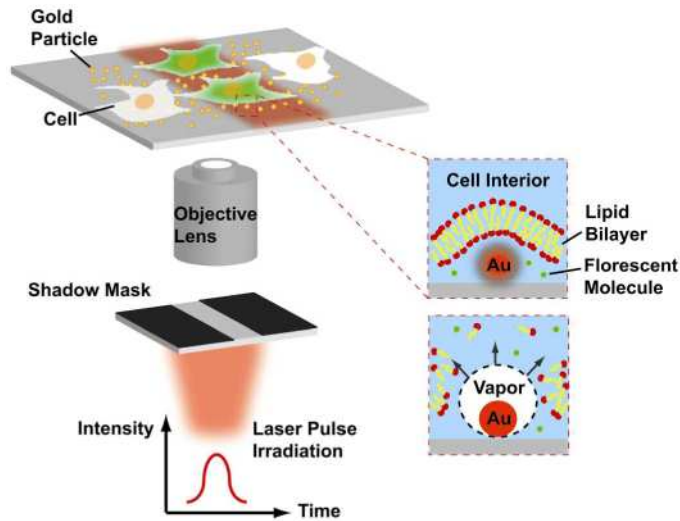


Fig. 1. Schematic of the device capable of image-patterned molecular delivery using a gold particle coated substrate.

### 3.2 Patterned laser irradiation and a time-resolved imaging system

Figure 2 illustrates the experimental setup. The laser source is the same one used for gold film annealing as described in 3.1. A shadow mask with a rectangular opening (2.3×4 mm) was placed in the laser beam path to cast the desired optical pattern. The laser pattern was imaged through an objective lens (40×, 0.6 NA) onto the device at a 25× reduction. Cell cultures were observed using an inverted microscope (Zeiss, AxioObserver) with phase contrast and epi-fluorescence capabilities. To capture the extremely short-lived cavitation bubbles induced by the pulsed laser (typically with a lifetime < 1 μs), a time-resolved imaging system was constructed. This included a high-speed Intensified CCD camera (Princeton Instrument, PI-MAXII), providing exposure times as short as 500 ps. A programmable delay between receiving the laser triggering signal and the camera shutter opening was set by the camera control unit. After the polarizing beam splitter, one arm of the laser beam was sent through a fluorescent dye cell (Exciton, LDS 698). The excited fluorescence pulse (wavelength centered around 698 nm) was coupled into a multimode fiber (Thorlabs, BFL37-600) and then sent through the microscope condenser to illuminate the sample, in synchronization with the camera shutter. A nanosecond time delay between the captured bubble image and the excitation laser pulse can be achieved by controlling the length of the optical fiber delay line.

### 3.3 Dye delivery efficiency and cell viability evaluations

HeLa and immortalized human embryonic kidney cells (HEK293T) were cultured in Dulbecco's Modified Eagle Medium (DMEM), supplemented with 10% fetal bovine serum (Hyclone), 50 mg/ml non-essential amino acids, 50 mg/ml penicillin/streptomycin, and 50 mg/ml sodium pyruvate. Cells were harvested and plated in a dish on top of a gold particle coated coverslip, fabricated by pulsed laser annealing. Cells were incubated overnight until about 90-100% cell confluence was reached. Cell density was measured and controlled to be around 3700 cells/mm<sup>2</sup> for HeLa and 4000 cells/mm<sup>2</sup> for HEK 293T. During laser pulsing, the cells were immersed in cell culture medium containing the membrane-impermeable fluorescent dye calcein (Invitrogen, 0.62 kDa) at 100 μM. After cavitation induction, the cell culture was washed with phosphate buffered saline (PBS, pH 7.4) and incubated in fresh

medium for 90 minutes at 37°C before adding propidium iodide (PI) at 5 µg/ml. PI is used as a dead cell indicator as it stains the DNA of dead cells and is excluded from viable cells. Cells were incubated in the presence of PI for another 30 minutes at room temperature and were washed with PBS, pH 7.4, before fluorescence imaging. Dye delivery efficiency was measured as the percentage of cells showing obvious calcein uptake within the laser irradiation pattern. Viability was calculated as the percentage of cells that were negative of PI staining within the laser irradiation pattern.

For multiplexed molecular delivery, the cell culture was first irradiated with the horizontal bar pattern to induce dextran-tetramethylrhodamine (Invitrogen, 40 kDa) uptake. Following a wash and change of medium, the same culture was irradiated with the two vertical bars to induce calcein uptake. The cell culture was then washed and checked for fluorescence. A concentration of 100 µM was used for both fluorescent molecules.

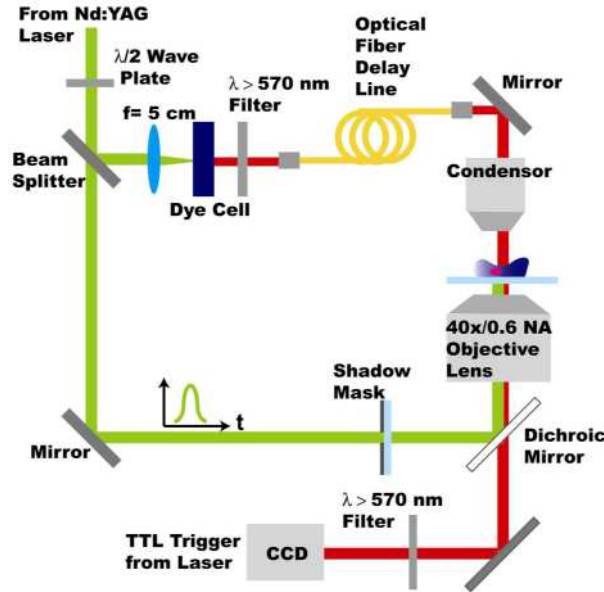


Fig. 2. Schematic of the experiment setup for light-patterned molecular delivery and the time-resolved imaging system used to capture the cavitation bubble dynamics.

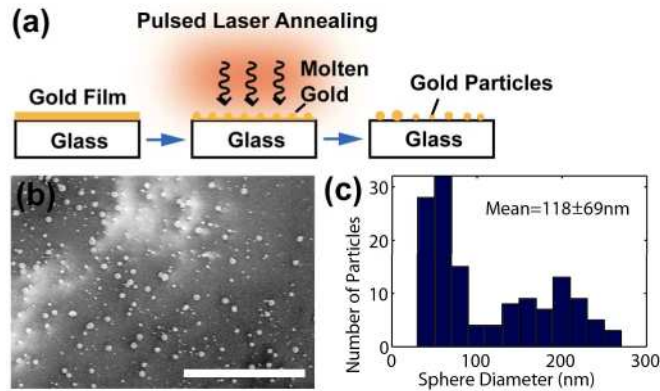


Fig. 3. Pulsed laser annealing of gold films. (a) Schematic of the formation of gold particles. (b) SEM images of the 10 nm gold film annealed at 49.5 mJ/cm<sup>2</sup>. (c) Measured particle size distribution. Bar=5 µm.

## 4. Results

### 4.1 Gold particle coated substrate generation by pulsed laser annealing of gold films

Pulsed laser annealing of metal thin films has been investigated [6,7]. It allows for large area annealing in a room temperature environment while minimizing substrate heating. This way the top layer can be effectively annealed even on a low-melting-point substrate, such as plastic [8]. During the laser pulse irradiation, the metal layer rapidly heats up. For metals which have poor wetting properties on the substrate (e.g. gold on SiO<sub>2</sub>), instability and capillary flow drive the molten thin film to break up into droplets and form metal particles as the droplets re-solidify. For 10 nm thick gold films, the measured particle diameter distribution showed two peaks (Fig. 3(c)). One centered around 50 nm and the other at around 200 nm, resulting in a mean particle diameter of 118 nm. The particle density obtained was 3.0 particles/ $\mu\text{m}^2$ . This corresponds to 300 particles per cell, assuming the area of a HEK293T fibroblast or HeLa is  $\sim 10 \times 10 \mu\text{m}$ .

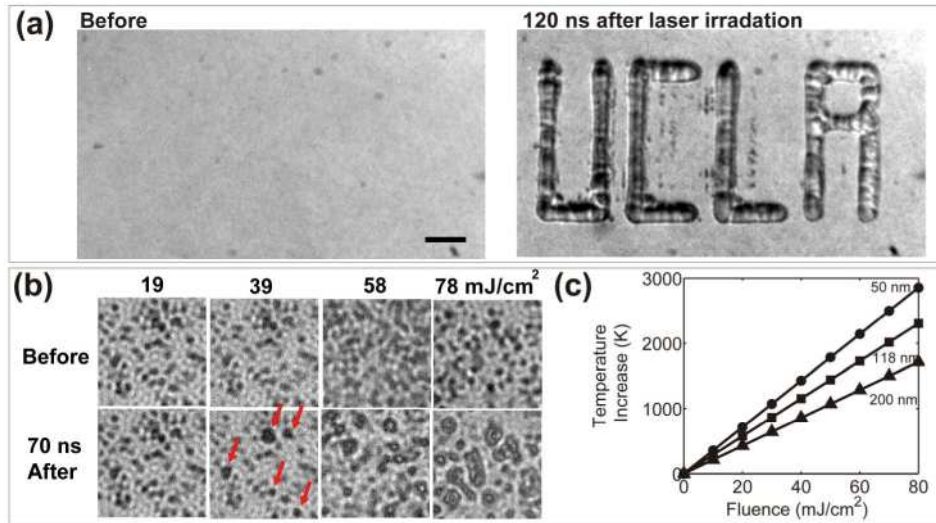


Fig. 4. Image patterned bubble nucleation. (a) Bubble pattern by irradiating a “UCLA” light pattern onto the substrate. Laser fluence = 153.5 mJ/cm<sup>2</sup>. Bar = 50  $\mu\text{m}$ . (b) Bubble nucleation (indicated by red arrows) was observed at laser fluences higher than 39 mJ/cm<sup>2</sup>. Field of view = 10 $\times$ 10  $\mu\text{m}$ . (c) Calculated temperature increase at the surface of the gold particle (50, 118 and 200 nm in diameter) at the end of the 6 ns laser pulse under various laser fluences.

### 4.2 Image patterned cavitation bubble nucleation

Noble metal particles exhibit large absorption cross sections in the visible and near-infrared range due to their surface plasmon resonance [9,10]. The energy of the collective electron oscillation is transferred to the lattice and rapidly heats up the particle and the liquid medium adjacent to the particle through thermal conduction [5]. The temperature range for bubble nucleation on the heated particle surface is characterized by the spinodal of water at atmospheric pressure, around 315 °C [11]. This criterion sets a minimum threshold for the laser fluence. Upon surpassing this threshold for cavitation bubble induction, the bubble volume is linearly proportional to the laser fluence [5].

To model this energy transduction process, we used Mie theory [12,13] to calculate the absorption coefficient,  $Q_{\text{abs}}$ , of gold spheres of different diameters in water. The refractive index of gold was taken from Johnson and Christy [14] with  $n_{\text{gold}} = 0.62 + 2.08i$  at  $\lambda_{\text{vacuum}} = 521 \text{ nm}$ . The refractive index of water was  $n_{\text{water}} = 1.33$ . We calculated  $Q_{\text{abs}} = 3.34$ , 2.14 and 1.65 for gold spheres of diameter 50 nm, 118 nm and 200 nm, respectively. To

simplify the analysis and yet obtain insightful solutions, we modeled the system as a gold sphere immersed in an infinite water medium. The temperature increase in the sphere due to the absorbed laser energy can be determined by solving the heat equation, Eq. (1):

$$\frac{\partial T}{\partial t} - \kappa \nabla^2 T = \frac{A}{\rho c_p} \quad (1)$$

where  $T$  is the temperature increase,  $\rho$  is the density,  $c_p$  is the specific heat, and  $\kappa$  is the thermal diffusivity of gold.  $A$  is the heat generation rate per unit time per unit volume and was modeled by Eq. (2) (assuming spatial and temporal homogeneous heat deposition within the particle):

$$A = \frac{(\pi R^2) Q_{abs}}{\frac{4}{3} \pi R^3} \cdot \frac{H}{\tau_{pulse}} = \frac{3 Q_{abs} H}{4 R \tau_{pulse}} \quad (2)$$

where  $H$  is the laser fluence,  $\tau_{pulse}$  is the laser pulsewidth, and  $R$  is the particle radius. Using the analytical solution obtained by Goldenberg and Tranter [15], the calculated temperature increase at the surface of the gold particle is linearly proportional to the irradiation laser fluence (Fig. 4(c)). The threshold fluence (300K temperature increase) is approximately 8.4, 10.4 and 14.0 mJ/cm<sup>2</sup> for particles of diameter 50 nm, 118 nm and 200 nm, respectively.

We experimentally verified the bubble generation using the time-resolved imaging system depicted in Fig. 2. To determine the threshold laser fluence for bubble nucleation, a 100×, 1.25 NA oil immersion objective lens was used to image the gold particle-coated substrate. As shown in Fig. 4(b), cavitation bubbles can be observed at laser fluences higher than 39 mJ/cm<sup>2</sup>. This measured threshold value is almost 4 times higher than the calculated value obtained from the analytic model. For more accurate modeling, the effect of the glass substrate on optical absorption as well as heat conduction (borosilicate glass has a higher thermal conductivity than water) cannot be ignored. To demonstrate image patterned bubble nucleation, a shadow mask with a “UCLA” pattern opening was used. The bubbles were nucleated around the gold particles in the irradiated area and coalesced with one another forming larger bubbles with the shape of the letters (Fig. 4(a)).

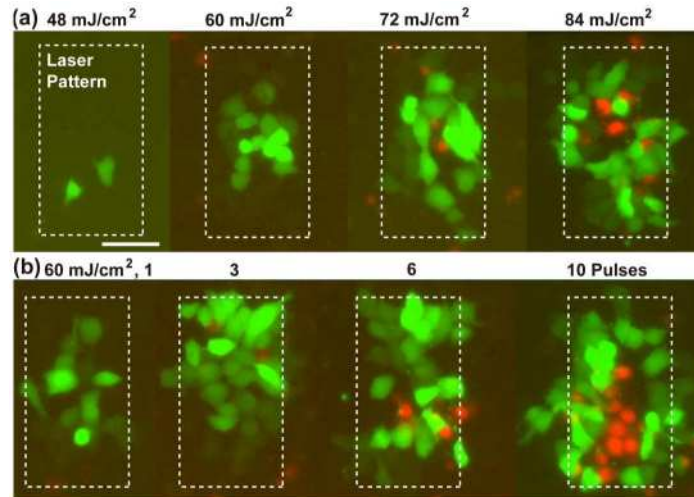


Fig. 5. Molecular delivery efficiency and cell viability assays in HeLa cells under (a) varying laser fluences (only irradiated with 1 pulse in each case) and (b) varying applied laser pulse numbers. Fluorescent images showing calcein (green) uptake within the laser irradiation pattern and propidium iodide (red) staining of dead cells. Bar = 50  $\mu$ m.

### 4.3 Image patterned molecular delivery into adherent cells

The efficiency of molecule delivery into cultured cells in general increases with irradiation laser fluence and the number of laser pulses applied. This can be rationalized by a larger pore formation on the cell membrane due to larger cavitation bubbles and the number of times the pores are induced. However, the disruption of the cell membrane needs to be kept at a minimum to avoid irreversible damage that leads to cell death [16]. We systematically varied the laser fluence and the applied pulse number to evaluate uptake efficiency and the corresponding cell viability. Figure 5 shows representative images of these assays. The laser irradiation pattern was measured to be  $90 \times 160 \mu\text{m}$ . To assess the effect of laser fluence, one laser pulse was applied in each case with fluence varying from 24 to  $84 \text{ mJ/cm}^2$ . In the other case, laser fluence was kept at a constant value ( $60 \text{ mJ/cm}^2$  for HeLa and  $36 \text{ mJ/cm}^2$  for HEK 293T) while the applied pulse number was increased in the order of 1, 3, 6 and then 10 pulses. Efficiency and viability results were measured and plotted in Fig. 6. For calcein uptake, the observed threshold fluence was around  $48 \text{ mJ/cm}^2$  for HeLa and  $36 \text{ mJ/cm}^2$  for HEK 293T. These values match well with the threshold laser fluence for bubble nucleation obtained experimentally. Higher laser fluences increased the number of cells loaded with calcein within the irradiated area as expected. A similar increase in uptake efficiency was also observed by increasing the applied pulse number. However, the efficiency reached a plateau for 6 and more laser pulses. This can be explained by the explosion of the cavitation bubbles detaching some of the particles from the substrate after each laser pulse. The particle is lost in the medium and the particle density on the substrate decreases, and hence the uptake efficiency ceases to increase. This phenomenon was also observed when imaging the cavitation bubbles on the substrate. The overall bubble density decreased with an increasing number of laser pulses. The highest efficiency and viability achieved in these assays were  $58.2 \pm 4.8\%$  (mean  $\pm$  standard deviation) efficiency with  $86.1 \pm 3.4\%$  viability in HeLa (number of experiments  $n=3$ ) and 98% efficiency with 90% viability in HEK 293T ( $n=1$ ). Both experiments used one laser pulse at  $84 \text{ mJ/cm}^2$ . These efficiency and viability values are comparable to that of a commercial automated scanning laser optoinjector [17]. In the optoinjector, a highly focused pulsed laser beam (wavelength 532 nm with a pulse duration of 0.5 ns) porates the targeted cell membrane. A pair of x-y galvanometer mirrors scans the focused laser spot across the cell layer to achieve large-area, patterned poration and transfection. In this optoinjection system, the optoinjection efficiency of Sytox Green (MW 0.9kDa) in HeLa cells with a single laser pulse was around 50% with above 80% cell viability at the critical laser fluence of  $60 \text{ nJ}/\mu\text{m}^2$ . The fluence level is about 100 times higher than that used in the gold particles coated substrate presented in this work ( $60 \text{ mJ/cm}^2$ ). The gold particles act as highly optical energy absorbing agent and decrease the energy threshold for inducing cavitation and the subsequent membrane poration. Hence a lower intensity, non-focused light pattern can be used to achieve large area, parallel permeabilization in a monolayer cell culture.

In Fig. 7, multiplexed molecular delivery was demonstrated on the device. The cell culture was irradiated with a double horizontal bar laser pattern in the presence of dextran-tetramethylrhodamine in the medium. After a wash, the cell culture was irradiated again with a double vertical bar laser pattern in a medium containing calcein to form the resultant multiplexed pattern. Within the field of view, four distinct groups of cells were present: cells loaded with both dextran-tetramethylrhodamine and calcein (4 corners of the square), ones with only dextran-tetramethylrhodamine (horizontal lines of the square), ones with only calcein (vertical lines of the square) and ones without any of these molecules (inside and outside of the square).

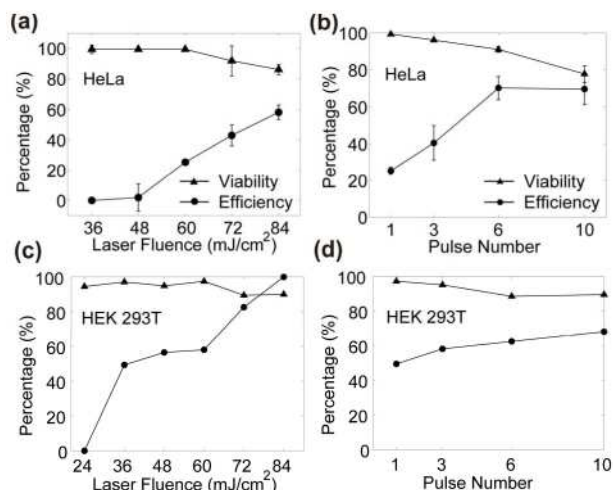


Fig. 6. (a,c) Calcein delivery efficiency and cell viability under varying laser fluences (only irradiated with 1 pulse in each case). (b,d) Efficiency and viability under varying applied laser pulse numbers at 60 mJ/cm<sup>2</sup> for HeLa (b) and at 36 mJ/cm<sup>2</sup> for HEK 293T (d). The viability and efficiency values are represented as mean  $\pm$  standard deviation. Number of experiments conducted are n=3 for HeLa and n=1 for HEK 293T.

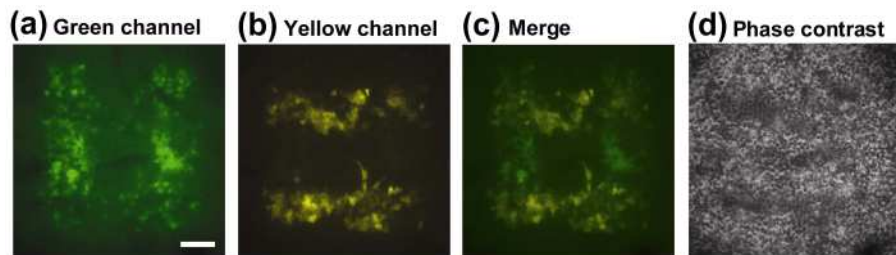


Fig. 7. Multiplexed dye delivery. (a) Calcein uptake was induced in the vertical bar area (green channel). (b) Dextran-tetramethylrhodamine uptake was induced in the horizontal bar area (yellow channel). (c) Delivery for both calcein and rhodamine was induced in the 4 corners of the square pattern in the cell culture. (d) Phase contrast image shows a confluent monolayer of viable HeLa cells that were imaged by immunofluorescence microscopy in panels (a-c). Bar = 100  $\mu$ m.

## 5. Discussion and conclusion

Methods for delivering molecules and genes into living cells have been highly sought after in biology. A device capable of light-patterned molecular delivery is described here. Successful delivery of fluorescent molecules was demonstrated in adherent cell culture. The targeted delivery area was controlled by a shadow mask. Delivery efficiencies can be as high as  $58.2 \pm 4.8\%$  in HeLa and 98% in HEK 293T for small molecules such as calcein. The threshold laser fluence observed necessary for calcein uptake was 48 mJ/cm<sup>2</sup> for HeLa and 36 mJ/cm<sup>2</sup> for HEK 293T, close to the experimentally found bubble nucleation threshold of 39 mJ/cm<sup>2</sup>. For larger molecules such as dextran-tetramethylrhodamine, we observed similar delivery efficiency (calculated by the number of cells loaded with the fluorescent molecule of interest divided by the total number of cells within the laser irradiation pattern). However, the average fluorescence intensity exhibited in cells was discernibly lower for dextran-tetramethylrhodamine compared to calcein. Judging from this observation, we think given the same cavitation condition inducing cell membrane poration, the average number of fluorescent molecules delivered per cell was lower for rhodamine compared to calcein. This could be due to the slower thermal diffusion speed of rhodamine, which allowed fewer molecules to diffuse across the transient pores during the time the pores remain open. To

estimate the physical size of the dye molecules, we calculate the Stokes radius,  $r_s$ , of an equivalent Einstein sphere using Eq. (3):

$$r_s = \frac{k_B T}{6\pi\eta D} \quad (3)$$

where  $k_B T = 4.14 \times 10^{-21}$  (J) at 300 K,  $\eta \equiv$  viscosity of water =  $10^{-3}$  (N·s·m<sup>-2</sup>) and  $D \equiv$  diffusion coefficient of the dye molecule. The calculated Stokes radius is around 5.5 nm for dextran-rhodamine and 0.7 nm for calcein respectively (Table 1). The delivery was also impeded by the location of the pores forming on the bottom side of the cell. Microfluidic trenches or structures could be utilized to facilitate the delivery and increase the efficiency for large molecule uptake. This device has the potential to achieve large-scale, light-patterned molecule and gene delivery into living cells.

**Table 1. Calculated Stokes radius of fluorescent dye molecules**

Molecule	Molecular weight (Da)	Diffusion coefficient, D, in water (m <sup>2</sup> /s)	Stokes radius, $r_s$ (nm)
Calcein	0.6k	$3.3 \times 10^{-10}$ (Yoshida 2000)	0.7
Dextran-tetramethylrhodamine	40k	$4 \times 10^{-11}$ (Peters 1984 for 62kDa Dextran molecules)	5.5

N. Yoshida, M. Tamura and M. Kinjo, *Single Mol.* **1**(4), 279-283 (2000).

R. Peters, *J. EMBO* **3**(8), 1831-1836 (1984).

### Acknowledgments

This project is supported by the NSF (CBET 0853500), the NIH Roadmap for Medical Research Nanomedicine Initiative (PN2EY018228), the Broad Center of Regenerative Medicine and Stem Cell Research at UCLA, and by the Prostate Cancer Foundation Challenge Award. Ting-Hsiang Wu and Sheraz Kalim contributed equally to this work.